Polarization Responses of a Solitary and Optically Injected Vertical Cavity Spin Laser

Benjamin R. Cemlyn, Ian D. Henning, Michael J. Adams, Edmund Harbord, Ruth Oulton, Ville-Markus Korpijärvi, and Mircea Guina

***Abstract*— The polarisation properties of a quantum well spin – vertical cavity surface emitting laser (spin – VCSEL), both without injection and with variable polarisation optical injection, are investigated experimentally and compared with the spin flip model (SFM). Without injection, we demonstrate two distinct types of VCSEL-pump response depending on the signs of the linewidth enhancement factor, birefringence and dichroism: firstly where the pump and VCSEL have the same sign of the ellipticity, and secondly where the VCSEL ellipticity, accompanied by the linear polarisation, switches sign. We show that by controlling the injected power, ellipticity or linear angle, near circular polarisation can be obtained. These responses both give insight into the electro-optical injected spin-VCSEL system, and have practical implications for the use of spin VCSELs in unique applications exploiting the ellipticity degree of freedom.**

***Index Terms*— VCSEL, spin, polarization, injection.**

I. Introduction

SPIN VCSELs – devices which utilise conservation of spin angular momentum in the electron-photon lasing processes – have been shown to possess a variety of unique characteristics. Properties such as threshold reduction [1], [2], spin amplification [3]–[5] polarisation control [5]–[8], and high frequency polarisation oscillations [9]–[12] have been demonstrated. These have raised awareness of the potential uses of spin lasers in future communications systems [13], [14]. Bistability and dynamics of the linearly polarised (LP) VCSEL modes with current [15], [16], temperature [17], or linear optical injection [18]–[27] have been investigated in recent years, due to their optical memory and logic applications. While the LP aspects have received considerable attention, the study of elliptic or circular injection into spin lasers, and the elliptic polarisation that results [28]–[31] is less well documented. The present contribution provides a link between these two sets of work. We conduct an in-depth investigation of injection of variable power, linear polarisation and elliptic polarisation into a spin VCSEL, both experimentally and theoretically. Through analysis of the electron spin, and the ellipticity of the injection and resultant VCSEL fields, we establish unique insight into the interaction of these parameters in both spin and non-spin lasers. Our investigations reveal unusual input-output ellipticity responses, and these are explained in terms of the spin VCSEL parameters via the SFM model. We demonstrate how these ellipticity responses can be altered and optimised, and finally we propose applications based on the ellipticity, to extend the current use of conventional VCSELs where the output is linearly polarised. Furthermore our investigation of the VCSEL polarisation is in accordance with a recent report [32] which highlights a common sign error for alpha in the spin VCSEL literature. This paper is organised in six sections. In section II we describe our experimental set up. In section III we describe the polarisation terms and the spin flip model (SFM). The experimental and modelled results are presented in section IV, and these are discussed with regard to future work in section V. The conclusions are in section VI.

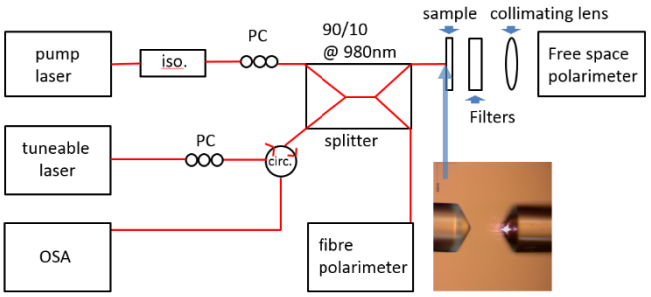

Fig. 1. Experimental set up. The splitter passed 59% of the 1300 nm light from the sample to the OSA, and from tunable laser to sample.

II. Experimental Set Up

Our experimental set up is shown in figure 1. We use a dilute nitride quantum well (QW) 1300 nm VCSEL wafer grown at Tampere University of Technology, Finland. Our VCSEL design utilises epitaxial top and bottom DBR mirrors formed from AlAs/AlGaAs $^1/_4$ wave layers (18 and 20.5 pairs respectively), and an active layer comprising 5 groups of GaInNAs QWs of 3 layers each, arranged at the antinodes of

Manuscript received May 5, 2019; revised August 16, 2019; accepted August 22, 2019. Date of publication September 9, 2019; date of current version October 1, 2019. This work was supported by the EPSRC, U.K., under Grant EP/G012458/1, Grant EP/M024237/1, and Grant EP/M024156/1. *(Corresponding author: Benjamin R. Cemlyn.)*

B. R. Cemlyn, I. D. Henning, and M. J. Adams are with the School of Computer Science and Electronic Engineering, University of Essex, Colchester CO4 3SQ, U.K. (e-mail: bencemlyn@blueyonder.co.uk).

E. Harbord is with the Department of Electrical and Electronic Engineering, University of Bristol, Bristol BS8 1UB, U.K.

R. Oulton is with the HH Wills Physics Laboratory, School of Physics, University of Bristol, Bristol BS8 1TL, U.K.

V.-M. Korpijärvi is with Okmetic Oy, FI-01510 Vantaa, Finland.

M. Guina is with the Optoelectronics Research Centre (ORC), Tampere University of Technology, FIN-33101 Tampere, Finland.

Color versions of one or more of the figures in this article are available online at http://ieeexplore.ieee.org.

Digital Object Identifier 10.1109/JQE.2019.2940041

the field profile. We have calculated the top and bottom mirror reflectivities as 99.6% and 99.8% respectively. The design is very similar to that described in [4], [7], [30], [31] except that it is has an additional two pairs of top layers.

The 8 × 8 mm cleaved wafer sample was bonded to a Si substrate and attached to a copper mount which was temperature controlled at 17 °C. The VCSEL wafer was optically pumped through the top mirror using a packaged 980 nm grating stabilised laser using Corning HI1060© optical fibre via a splitter, and a polarisation controller (PC). This is a very similar experimental arrangement to that reported previously [4] except that instead of a cleaved fibre, here we used a high NA lens-ended fibre, enabling a minimum spot size of approximately 2.5um FWHM. This enabled much better control of the photopumped area that defines the lasing region of the VCSEL. The lensed fibre was positioned by a dual manual/piezo-controlled stage. A splitter enabled a small proportion of the pump light in the fibre path to be directed to a fibre polarimeter to monitor the pump polarisation. The VCSEL output coupled back into the fibre along the return fibre path passed through the splitter and circulator into an optical spectrum analyser (OSA). A 1300 nm tunable laser (TL) of resolution 0.01 nm with a second PC was used to inject polarisation controlled light via the circulator and splitter. Reflection of the tunable laser from the sample surface, and VCSEL emission were both coupled into the fibre return path which allowed simultaneous observation of their spectra on the OSA. Thus the TL could be aligned to the resonance of the VCSEL lasing mode at 1300 nm. The output from the rear of the sample was filtered to remove the pump light and coupled into a free space polarimeter. This arrangement allowed separate measurement of the polarisations of the VCSEL emission and injected signal. When biased significantly below threshold, the injection polarisation could be measured directly, and this was verified to be the same without the VCSEL wafer in place, demonstrating that the single pass birefringence and dichroism of the wafer was small. With the VCSEL optically pumped above threshold, the resultant polarisation of the injected VCSEL could also be measured. Using this arrangement, the pump polarisation was recorded simultaneously with the native or injected VCSEL polarisation.

The VCSEL sample was optically pumped whilst observing the spectra at high resolution at different wafer positions, and a threshold pumping power of ∼200 mW was required for lasing, similar to figures published in [4], [7], [8]. The need for high pump power is largely due to the low absorption in the QW active region and single-pass pumping, as discussed in [4] and demonstrated in [33]. Once threshold had been identified, the VCSEL was biased at approximately 10% above the lasing threshold throughout subsequent measurements. A small bias above threshold has been shown to produce more useful polarisation responses [4]. Depending on the focus from the lensed-ended fibre, we observed distinct narrow and broad spectral peaks spaced between approximately 0.05 nm and 0.7 nm from each other. These were thought to be symptomatic of different spatial modes, and separate tests using a free space optical set up with an infra red camera confirmed this. By controlling the focusing, we isolated lasing in a short wavelength, narrow spectral width peak, and found that the polarisation response of the VCSEL then gave results which were in good agreement with the spin flip model (SFM).

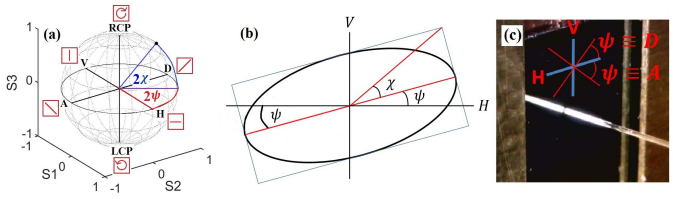

Fig. 2. Polarisation parameters. (a): Ellipticity (χ) and major axis angles (ψ) on the Poincare sphere, with vertical (V), horizontal (H), diagonal (D) and antidiagonal (A) ψ polarisations; (b) Polarization ellipse defining ψ and χ (c) Wafer alignment with cleaved axis aligned to H, V (blue). The D, A example ψ values (red) show the degeneracy of ψ on the left and right sides of the diagram i.e. that ψ has a range of π.

III. Polarisation Terms and the Spin Flip Model

The polarisation is measured experimentally using the Stokes S1,2,3 parameters on the Poincare sphere. These are defined by the major axis angle of the polarisation ellipse ψ, and the ellipticity angle χ, as shown in figure 2a,b and equations (1)-(4). Using (1) and (2), ψ can be derived with (5) using the 4-quadrant atan2 function, noting that both S3 and S2 are signed values. As the Stokes S1 and S2 parameters define ψ, we present the polarisation here via only the VCSEL major axis angle ψ_{VCSEL} and Stokes ellipticity $S3_{VCSEL}$. These are measured in terms of the pump polarisation ellipticity $S3_{pump}$, the injection ellipticity $S3_{inj}$ and the injection angle ψ_{inj}.

$$S1 = \cos 2\chi \cos 2\psi \tag{1}$$

$$S2 = \cos 2\chi \sin 2\psi \tag{2}$$

$$S3 = \sin 2\chi \tag{3}$$

$$S1^2 + S2^2 + S3^2 = 1 \tag{4}$$

$$\psi = \frac{1}{2}\tan^{-1}\frac{S2}{S1} \tag{5}$$

We use the SFM with injection, originally presented in [34], without any consideration of misalignment between the axes of birefringence and dichroism (which has been investigated in e.g. [32], [35], [36]). The SFM in terms of the linearly polarised complex fields $\tilde{E}_x$, $\tilde{E}_y$, is given in equations (6) to (9):

$$\frac{d\tilde{E}_x}{dt} = \kappa(1+i\alpha)\left[(N-1)\tilde{E}_x + im\tilde{E}_y\right] - \left(\gamma_a + i\left(\gamma_p + \Delta\omega\right)\right)\tilde{E}_x + \kappa_{inj}\tilde{E}_{inj,x} \tag{6}$$

$$\frac{d\tilde{E}_y}{dt} = \kappa(1+i\alpha)\left[(N-1)\tilde{E}_y - im\tilde{E}_x\right] + \left(\gamma_a + i\left(\gamma_p - \Delta\omega\right)\right)\tilde{E}_y + \kappa_{inj}\tilde{E}_{inj,y} \tag{7}$$

$$\frac{dN}{dt} = -\gamma\left[N\left(1+|\tilde{E}_x|^2+|\tilde{E}_y|^2\right) - (\eta_+ + \eta_-) + im\left(\tilde{E}_y\tilde{E}_x^* - \tilde{E}_x\tilde{E}_y^*\right)\right] \tag{8}$$

$$\frac{dm}{dt} = -\gamma_s m - \gamma\left[m\left(|\tilde{E}_x|^2+|\tilde{E}_y|^2\right) - (\eta_+ - \eta_-) + iN\left(\tilde{E}_y\tilde{E}_x^* - \tilde{E}_x\tilde{E}_y^*\right)\right] \tag{9}$$

$\tilde{E}_x$ and $\tilde{E}_y$ are usually aligned to the horizontal (H) and vertical (V) axes, respectively. κ is the field decay rate, γ_a and γ_p the linear dichroism and birefringence, γ and γ_s the electron recombination and spin rates, and α is the linewidth enhancement (Henry) parameter. $\tilde{E}_{inj,x}$ and $\tilde{E}_{inj,y}$ are the complex injection fields, κ_{inj} the injection rate and $\Delta\omega$ the detuning between VCSEL and injection fields, which is here set to zero. η_+, η_- are the spin up, down pumping parameters, N is the total (spin up and down) electron density and m is the difference in spin up, down electron populations. The hole relaxation rate is effectively instantaneous [7]. The pump ellipticity $S3_{pump}$ is derived from η_+, η_- using:

$$S3_{pump} = \frac{\eta_+ - \eta_-}{\eta_+ + \eta_-} \tag{10}$$

The generation of the Stokes parameters from the complex VCSEL fields $\tilde{E}_x$, $\tilde{E}_y$ is detailed in Appendix A1. The complex injection fields $\tilde{E}_{inj,x}$, $\tilde{E}_{inj,y}$ in (6) and (7) are generated from the defined $S3_{inj}$, ψ_{inj} as per Appendix A2. We solve equations (6)-(9) in the time domain using a variable time-step Runge-Kutta method via the Matlab™ ode45 function. The time series were propagated for 80ns, with the polarisation averaged over the last 30ns where the time series converged to steady state solutions.

IV. Experimental and Modelled Results

A. Solitary Spin VCSEL

The sample used here is the same design as that previously reported in [4], [7], [30], [31] but with the addition of two mirror pairs. In practice this did not result in any significant changes in measured output-pump characteristics; therefore we used values we calculated in [4] of κ (68.5 ns^{-1}) and the scaling above threshold of the pump rate η to the pump rate P/P_{th} (143%). The material parameters (derived from published experimental measurements of our material) are similarly unchanged, with $\gamma = 1\ ns^{-1}$, $\gamma_s = 64\ ns^{-1}$ and $\alpha = -2$ (note sign). For this unprocessed wafer we anticipate small linear dichroism γ_a and birefringence γ_p. To begin with we performed detailed experimental characterisation of the elliptic and linear polarisation of the solitary photopumped sample i.e. $\psi_{VCSEL}, S3_{VCSEL}$ in terms of $S3_{pump}$ (figures 3a-d). We then fitted these measurements to the SFM through variation of γ_a and γ_p, deducing values of $\gamma_a = 0.1\ ns^{-1}$ and $\gamma_p = 2\ ns^{-1}$. Next we note that care needs to be taken over the sign of the α parameter as it appears in the SFM equations, which has been highlighted recently [32]. In a similar vein we also consider the influence of the signs of the birefringence and dichroism. We tested this with examples of two distinct types of experimental polarisation response that are found in the SFM without injection. The first type of response is plotted in figure 3e and characterised by an S–shaped VCSEL-pump ellipticity curve, where $S3_{VCSEL}$ and $S3_{pump}$ are of the same sign, and there is a small rotation i.e. change in ψ_{VCSEL} (figure 3f). This type relates to responses and wafer samples in [4], [7], and is modelled with values of γ_a and γ_p, of 0.05 ns^{-1} and $-0.35\ ns^{-1}$ respectively. This type of response is commonly found in the spin VCSEL literature [3]–[8] and usually characterises spin amplification of the pump. A second type, found in the sample used in this work is characterised by a switch in $S3_{VCSEL}$ to the opposite sign of $S3_{pump}$ (figure 3a,c), accompanied by a large rotation of ψ_{VCSEL} of nearly $\pi/2$ at each switching point (figure 3b,d). This type of response has been investigated in [37] and is shown to be due to switching between two stable solutions of the SFM equations, although the large rotation of ψ_{VCSEL} with $S3_{pump}$ does not appear to have been reported previously.

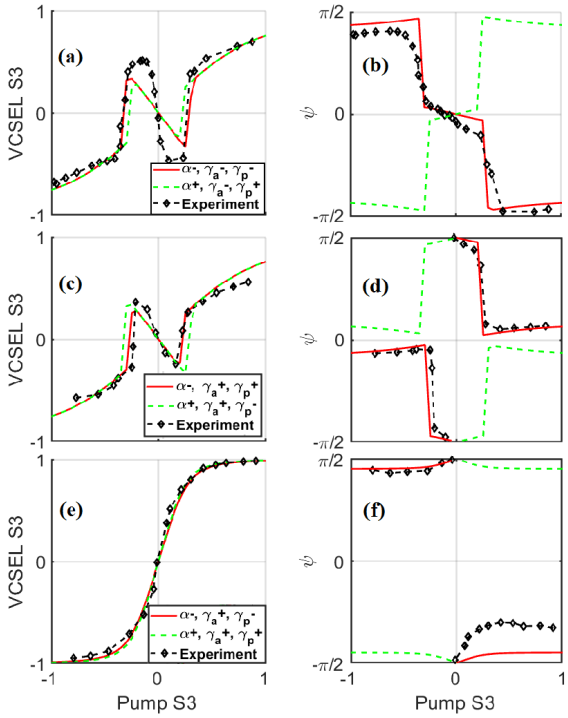

Fig. 3. Experimental and SFM polarisation responses with signed values of α, γ_a and γ_p: (a), (b) Switching response with greater gain in H axis ($\gamma_a{}^-$); (c), (d) Switching response with greater gain in the V axis ($\gamma_a{}^+$); (e), (f) S-shaped response with $\gamma_a{}^+$. The remaining two of eight SFM sign combinations (from $\alpha^{+/-}$, $\gamma_a{}^{+/-}$ and $\gamma_p{}^{+/-}$) which give an S-shaped response with $\gamma_a{}^-$ are not shown, as a suitable experimental example was not available.

Figure 3 shows that with negative α in the SFM, the switching response occurs when the dichroism γ_a and birefringence γ_p are of the same sign (red lines, figure 3a,c), and the S-shaped response occurs when they are of opposite sign (red lines figure 3e). Conversely for positive α, the switching response occurs when γ_a and γ_p are of opposite signs (green lines, figure 3a,c) and the S-shaped response occurs when they are of the same sign (green line figure 3e). This holds for all except very small values of γ_a and γ_p, hence care is needed in that circumstance. Changing only the signs of α (and γ_a, γ_p) to maintain the type of polarisation response is seen to change the $S3_{VCSEL}$ values only marginally (figure 3a,c,e) however the SFM polarisation paths $\psi_{VCSEL}(S3_{pump})$ change dramatically (figures 3b,d,f), revealing a match in the sign of ψ_{VCSEL} between the experiment (black lines figure 3b,d,f) and SFM only when α is negative (red lines). Moreover for other sign combinations, or variation of these parameters, ψ_{VCSEL} and $S3_{VCSEL}$ are not well reproduced. When focussing solely

on the VCSEL ellipticity, which is common for spin lasers, the sign of α in the SFM is not critical. However this study of ψ_{VCSEL} reveals α must be negative, and thus, care must be taken in formulism of the SFM [32], [34], to ensure α appears appropriately signed.

The two experimental examples of the switching responses in figure 3a,b and 3c,d were achieved by rotating the wafer planar axes by 90 degrees. There is a noticeable difference in the $S3_{VCSEL}$ paths between these two results, with figure 3c,d better reproduced by the SFM, but this is representative only of the small variation in ellipticity responses observed in this wafer and unrelated to the axis orientation. Noting the signs in equations (6) and (7), positive γ_a and γ_p give higher gain and frequency for the y polarisation and lower values in the x polarisation. As the physical H,V axes have been switched between these two orientations, the signs of both γ_a and γ_p are correspondingly reversed in the SFM. Despite the flexibility that the SFM sign convention gives for the *absolute* signs of γ_a and γ_p depending on orientation, the *relative* signs of γ_a and γ_p are physically significant, as the spin VCSEL system will display very different behaviour with higher gain and frequency in the same axis than in different axes, as shown above. Both signed [35] and absolute [38] frequency differences between the orthogonal [110] and $[1\bar{1}0]$ crystalographic axes for QW spin-VCSELs have been recently published. In [34] both negative and positive frequency splitting between [110] and $[1\bar{1}0]$ was seen, and in each case the gain splitting was of opposite sign to the frequency splitting. However the existence of the switching response in figure 3 and [37] indicate that (with a negative α) the gain and frequency splitting (which broadly define γ_p and γ_a) can have the same sign.

B. Spin VCSEL With Optical Injection

We applied optical injection to our wafer and examined the VCSEL polarisation $S3_{VCSEL}$, ψ_{VCSEL} as a function of pump and injection ellipticity $S3_{pump}$, $S3_{inj}$ and injection angle ψ_{inj}. Hereon we adopt a common set of SFM parameters $\gamma_a = +/-0.1\ ns^{-1}$, $\gamma_p = +/-2\ ns^{-1}$ and $\alpha = -2$, with any variation being noted. The $\gamma_{a,p}$ signs (from wafer orientation) are also noted. Although the injection power was 2 mW, the optical coupling efficiency into the VCSEL mode is expected to be small, and will be sensitive to the fibre position. We found that an injection rate κ_{inj} between 0.015κ and 0.04κ produced a good SFM match to the range of experimental results (noted for each experiment below). This range of κ_{inj} values is an order of magnitude lower than those in [29]–[31], which used a different experimental set up, including higher pump rate and injection power. In figure 4 the VCSEL polarisation was recorded with swept $S3_{pump}$ as in figure 3, but with fixed $S3_{inj}$ of zero (figure 4(a),(c)) and $S3_{inj} = \sqrt{1/2}$ (figure 4(b),(d)), together with four equally spaced angles of ψ_{inj} i.e. H,V, diagonal (D) and antidiagonal (A). The ${\gamma_{a,p}}^+$ orientation was used. The experimental result for $S3_{inj} = 0$ shows the switching has been suppressed and the VCSEL ellipticity is increased for $\psi_{inj} \equiv A$ and reduced for $\psi_{inj} \equiv D$ (figure 4a). It is also increased somewhat for $\psi_{inj} \equiv V$ and decreased somewhat for $\psi_{inj} \equiv H$. The same trend is found

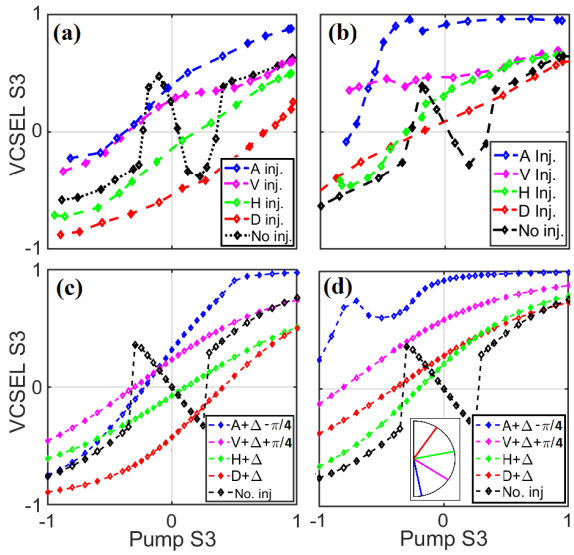

Fig. 4. VCSEL Stokes S3 parameter versus pump S3 with injection angles horizontal ($H, \psi_{inj} = 0$), vertical ($V, \psi_{inj} = \pi/2$), diagonal ($D, \psi_{inj} = \pi/4$) and antidiagonal ($A, \psi_{inj} = -\pi/4$) (a), (b) experiment and (c), (d) SFM. $S3_{inj}$ is zero (a), (c) and $\sqrt{1/2}$ (b) (d). The ${\gamma_{a,p}}^+$ orientation was used. The SFM Δ parameter is a rotation of $\pi/16$. The SFM injection rate was $\kappa_{inj}/\kappa = 0.025$.

for $S3_{inj} = \sqrt{1/2}$ in figure 4b. This indicates that there is an angle between A and V that maximises the ellipticity, and an angle between D and H that minimises it.

In figure 4b it is seen that a VCSEL ellipticity close to $+1$ is found for A injection, which is above the injection ellipticity of 0.71, and this is achieved even for zero or negative $S3_{pump}$. This constitutes spin amplification of the injection. In figure 4a, a negative or positive $S3_{VCSEL}$ is produced with $S3_{inj} = 0$, even for linear pumping, which constitutes spin generation (in this isolated system). Comparing the experiment to the SFM, we find that this unusual behaviour can be reproduced well. Figures 4c,d show a reasonable match with again four equally spaced angles ψ_{inj}, although the closest results to the experiment were found with an additional rotation Δ of $\pi/16$ from HVAD, with the A and V angles switched, as per figure 4c,d legend and 4d inset.

The response of $S3_{VCSEL}$ to injection ellipticity, ψ_{inj} in figure 4 was investigated further by taking a finer step of ψ_{inj}, with linear pump and injection ellipticity, shown in figure 5. The experimental response (figure 5a) in the same ${\gamma_{a,p}}^+$ orientation as figure 4 shows a positive peak in $S3_{VCSEL}$ for ψ_{inj} between V and A, and a negative peak in $S3_{VCSEL}$ for ψ_{inj} between V and D. This accords with the $S3_{VCSEL}(\psi_{inj})$ values in figure 4. The equivalent response in the ${\gamma_{a,p}}^-$ orientation ("orientation 2") is also shown, together with the modelled responses in figure 5b. The angle ψ_{inj} that maximises $|S3_{VCSEL}|$ is closer to the higher frequency axis - V for the ${\gamma_{a,p}}^+$ orientation, and H for the ${\gamma_{a,p}}^-$ orientation. This peak in $|S3_{VCSEL}|$ for linear pumping and linear injection has been demonstrated before in the SFM in [29] figure 16c. Only a negative $S3_{VCSEL}$ peak is shown in [29], as the angular parameter θ_p is used there,

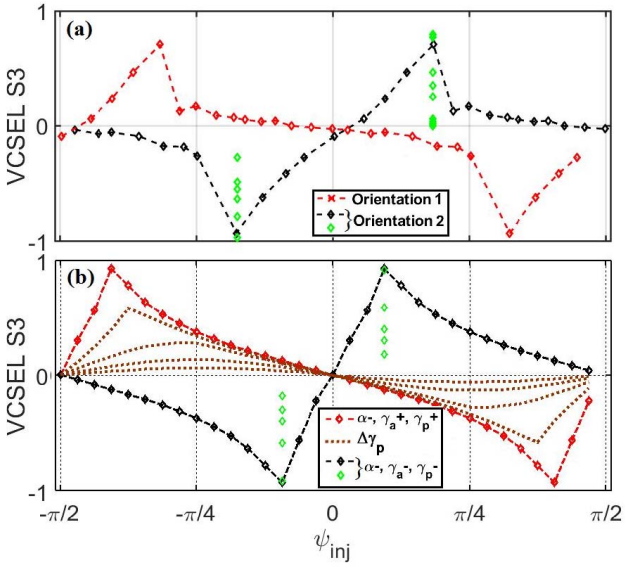

Fig. 5. VCSEL S3 versus ψ_{inj} for the case of linear pump and injection ellipticity; (a) Experimental $S3_{VCSEL}$ (b) SFM $S3_{VCSEL}$. κ_{inj} is $0.015 \times \kappa$ (red, black and brown lines) and $0.015, 0.02, 0.03, 0.04, 0.06 \times \kappa$ with decreasing S3 magnitude (green markers). γ_p varies (four brown dotted lines) as 0.1, 0.5, 1 and 1.5 ns^{-1} with increasing S3 magnitude.

which has half the polarisation range of ψ. The ellipticity peak is dependent on a particular ratio of injection rate to pump rate, or correspondingly injection field to VCSEL field. This is demonstrated in figure 5a from variation of pump power (green markers), giving an $S3_{VCSEL}$ range from nearly zero to $+/-1$. This could also achieved by variation of the injection power in the experiment. A similar range is shown using the SFM figure 5b from variation of κ_{inj}/κ. By testing the SFM response for the sign of α we confirm agreement with the experiment is only for negative values.

To examine in more detail the $S3_{VCSEL}(\psi_{inj})$ behaviour with the SFM, we firstly note from equation (A3) of Appendix A1 that S3 is written in terms of the phase difference ϕ and absolute field magnitudes as (11).

$$S3 = -2|\tilde{E}_x||\tilde{E}_y| \sin\phi / \left(|\tilde{E}_x|^2 + |\tilde{E}_y|^2\right) \tag{11}$$

For the case $S3_{inj} = 0$ here, $|\tilde{E}_{inj,x}| = \cos(\psi_{inj})$, $|\tilde{E}_{inj,y}| = \sin(\psi_{inj})$. We find that for small γ_a, γ_p the injection x,y field magnitudes fully control the VCSEL x,y field magnitudes, except with very small injection magnitudes. Therefore $|\tilde{E}_x| \propto \cos(\psi_{inj})$, $|\tilde{E}_y| \propto \sin(\psi_{inj})$ and if the phase remains fixed, using this in (11) we find that S3 is sinusoidal with ψ_{inj} as (12).

$$S3 \propto \pm \cos\left(\psi_{inj}\right) \sin\left(\psi_{inj}\right) \propto \pm \sin(2\psi_{inj}) \tag{12}$$

This is found in the SFM with small γ_p and γ_a, as shown by the lowest magnitude S3 brown line in figure 5b. Under these conditions the VCSEL is acting like a waveplate, viz. fixing the x,y phase difference, whilst the injection angle controls the relative x,y magnitudes and subsequent S3. As the fields are positive and real in (11), $0 \leq \psi_{VCSEL} \leq \pi/2$ so the sign choice from the phase gives the positive and negative S3 range. This is equivalent to removing the sign choice and accounting for the phase in ψ_{inj}, giving $-\pi/2 \leq \psi_{inj} \leq \pi/2$. For these SFM parameters, the phase is fixed close to $0, +/-\pi$ giving a small |S3|, but we find for small η and κ_{inj} it approaches $+/-\pi/2$, giving S3 approaching LCP,RCP. With the standard η and κ_{inj}, but increasing γ_p to the expected physical level of 2 ns^{-1}, we find the phase starts to vary, and also $|\tilde{E}_x|, |\tilde{E}_y|$ are no longer purely sinusoidal with ψ_{inj}. Consequently the |S3| peak becomes larger and skews towards the higher frequency axis (brown dotted lines figure 5b). This skewing, together with the S3 dependence on injection/pump rate, can be understood from the steady-state SFM with circular solutions. Substituting the LCP conditions $\tilde{E}_y = i\tilde{E}_x$ in (6) and $\tilde{E}_x = -i\tilde{E}_y$ in (7), assuming negligible γ_a gives

$$\kappa(1+i\alpha)[N-1-m]\tilde{E}_x - i\gamma_p\tilde{E}_x = -\kappa_{inj}\tilde{E}_{inj,x} \tag{13}$$

$$\kappa(1+i\alpha)[N-1-m]\tilde{E}_y + i\gamma_p\tilde{E}_y = -\kappa_{inj}\tilde{E}_{inj,y}. \tag{14}$$

Equations (13) and (14) define the injection magnitude for this circular solution as:

$$\kappa_{inj} = -\left[\kappa(1+i\alpha)(N-1-m) - i\gamma_p\right]\frac{\tilde{E}_x}{\tilde{E}_{inj,x}} \tag{15}$$

$$\kappa_{inj} = -\left[\kappa(1+i\alpha)(N-1-m) + i\gamma_p\right]\frac{\tilde{E}_y}{\tilde{E}_{inj,y}} \tag{16}$$

Variation from this optimum rate means the circular solutions do not hold, and the ellipticity will reduce as seen by the results in green, figure 5. Finally, from the ratio of (13) and (14):

$$\frac{\tilde{E}_{inj,x}}{\tilde{E}_{inj,y}} = \frac{\left[\kappa(1+i\alpha)(N-1-m) - i\gamma_p\right]}{\left[\kappa(1+i\alpha)(N-1-m) + i\gamma_p\right]}\frac{\tilde{E}_x}{\tilde{E}_y} \tag{17}$$

Equation (17) shows that as $\gamma_p \to 0$, the injection ratio $\tilde{E}_{inj,x}\Big/\tilde{E}_{inj,y}$ approaches unity for this circular polarisation condition of $\left|\tilde{E}_x\right| = |\tilde{E}_y|$ i.e. $\psi_{inj} = +/-\pi/4$. For finite positive (negative) γ_p, $\tilde{E}_{inj,x}\Big/\tilde{E}_{inj,y}$ reduces(increases) from unity, and the S3 peak in ψ moves towards the higher frequency axis in both cases. This simplified analysis indicates in terms of the $\tilde{E}_x, \tilde{E}_y$ magnitudes indicates why the S3 peak moves towards the higher frequency axis, but further analysis would be required to understand the phase variation (noted above) which also controls this process.

With the effect of ψ_{inj} now determined, the dependence of the $S3_{VCSEL}\left(\psi_{inj}\right)$ relation on the spin relaxation rate γ_s is now investigated in the SFM with finite $S3_{inj}, S3_{pump}$ of 0.38, and with two values of γ_p (figure 6). In figure 6a, $S3_{VCSEL}$ increases with reducing γ_s, as the resultant increasing spin polarisation exerts greater control of the resultant ellipticity. However the ellipticity peak close to the RCP axis occurs almost independently of γ_s. Indeed, the SFM results in figure 5b and [29] for linear pumping are found to change negligibly if $\gamma_s = \infty$, as there is no differential electron spin $\uparrow, \downarrow$ excitation from the pump in that case. In figure 6b, the same results are shown, but with reduced birefringence. The VCSEL ellipticity is now principally controlled by the pump and injection ellipticity and shows reduced dependence on ψ_{inj}. With smaller γ_p (or α) we also observe that any

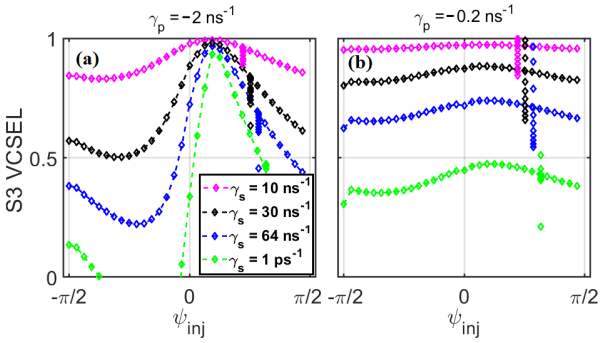

Fig. 6. SFM $S3_{VCSEL}$ with ψ_{inj} for, with finite $S3_{inj}$, $S3_{pump}$ of 0.38, and $\kappa_{inj} = 0.015$. The $\gamma_{a,p}{}^{-}$ orientation is used (c.f. figure 5 black line) (a) $\gamma_p = -2$ ns^{-1} (b) $\gamma_p = -0.2$ ns^{-1}. The vertical markers show variation of κ_{inj} from 0.015 to 0.06 × κ as per figure 5.

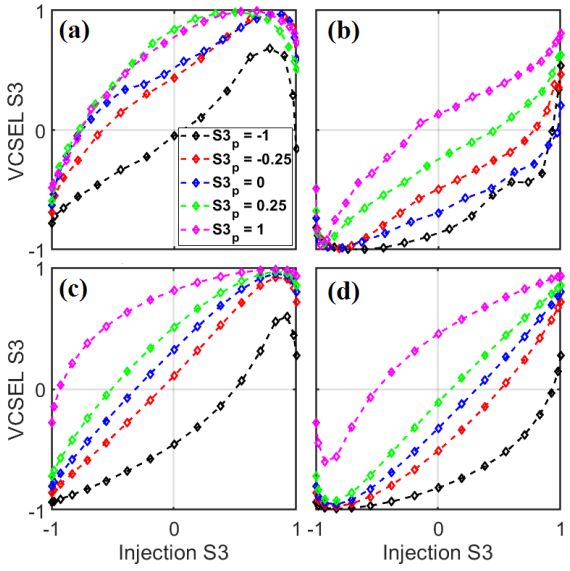

Fig. 7. VCSEL S3 versus injection S3 (a) Experimental, $\psi_{inj} \equiv A$, (b) Experimental, $\psi_{inj} \equiv D$, (c) SFM, $\psi_{inj} = A - 3/32\pi$, (d) SFM, $\psi_{inj} = D + 3/32\pi$. γ_p is $+2$ ns^{-1}. The SFM injection rate was $\kappa_{inj}/\kappa = 0.04$. The legend in 7a applies to plots (a)-(d), with the $S3_p$ denoting $S3_{pump}$.

oscillation in time between the H, V fields is more strongly damped. This accords with the polarisation oscillations that are observed for high birefringence in some cases [9]–[11]. For low γ_s, where the differential spin populations become much more significant and therefore control the ellipticity, the $S3_{VCSEL}(\psi_{inj})$ relation is almost flat.

We now focus on the VCSEL output, vs. injected input ellipticity transfer characteristics of this system. Figure 7a-d shows the $S3_{VCSEL}(S3_{inj})$ relation in the experiment and that from the SFM with $\gamma_{a,p}{}^{+}$ signs, for $\psi_{inj} \equiv A$ and $\psi_{inj} \equiv D$, giving a generally positive and negative $S3_{VCSEL}$ respectively. Note the symmetry of these results, which follows from the negligible (zero) circular anisotropies in the experiment (SFM). The pump is varied from LCP to RCP ($S3_{pump} = -1$ to $+1$). A good general fit of model to experiment is obtained by using a small shift of $\psi_{inj} = A - 3/32\pi$ and $\psi_{inj} = D + 3/32\pi$ in the SFM. This is consistent with the small

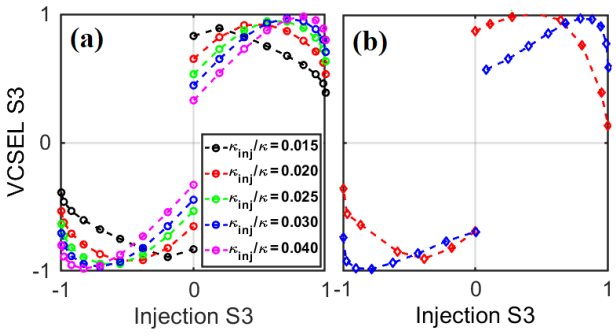

Fig. 8. VCSEL S3 versus injection S3 with linear pumping and varying injection magnitude (a) SFM ($\gamma_p = 2$ ns^{-1}) (b) experiment, with higher (blue) and lower (red) injection coupling.

ψ_{inj} shift in figure 4, and the ellipticity peaks in figure 5, which are somewhat closer ($\sim 3/32\pi$) to the V axis in the SFM than in the experiment. These small differences in experimental to modelled results can be expected considering the relative simplicity of the model. The $S3_{VCSEL}(S3_{inj})$ relation is distinctly nonlinear, with $S3_{VCSEL}$ peaking at $\sim +/-1$ for $S3_{inj} \sim +/-0.9$ and reducing thereafter. The VCSEL ellipticity is maximised when $S3_{pump}$ is of the same sign as $S3_{VCSEL}$, but shows relatively little difference between $S3_{pump}$ of $+/-0.25$ and $+/-1$. This can be ascribed to the near-saturation of $S3_{VCSEL}$ with $S3_{pump}$ seen in figures 3,4 and in e.g. [4].

The position of the ellipticity peak, together with the general shape of the $S3_{VCSEL}(S3_{inj})$ relation is seen to change with injection strength, shown in figure 8a,b, at linear pumping, and $\gamma_{a,p}{}^{+}$ orientation. Separate signed ψ_{inj} (i.e. A, D) for $S3_{inj}$ $-/+$ are used here, hence the discontinuity at $S3_{inj} = 0$. At linear injection, $S3_{VCSEL}$ peaks at $\kappa_{inj}/\kappa = 0.015$ and decreases with increasing injection ratio, in accordance with the results in figure 5 (green markers there).

Noting the reduced sensitivity of $S3_{VCSEL}$ to ψ_{inj} with reduced birefringence in figure 6b, the SFM $S3_{VCSEL}(S3_{inj})$ relation is shown with γ_p of 0.2 ns^{-1}, along with $S3_{pump}$ of +0.25,0.38 in figure 9a,b respectively. The expected physical γ_s value of 64 ns^{-1} is again used. An arbitrary value of ψ_{inj} of +0.5 (radians) is also used, due to the relative insensitivity of this parameter here. The solitary $S3_{VCSEL}$, without injection (black line), is now significantly higher than the figure 3 results due to the reduced birefringence, which is discussed in [4], [36], [39]. The shape of the $S3_{VCSEL}(S3_{inj})$ relations and movement of the peak with κ_{inj} are similar to figure 8, except the $S3_{VCSEL}$ values are much elevated (note the reduced plot ranges), and furthermore this result is not sensitive to ψ_{inj}.

V. Discussion and Future Work

We have examined experimentally and theoretically the principal types of pump-VCSEL ellipticity response in the solitary QW spin-VCSEL, and how these depend on the relative signs of α, γ_a and γ_p. Analysis of the linear polarisation angle ψ_{VCSEL} suggests that a negative sign of α should be used in the current formulism of the SFM, in accordance with a recent report.

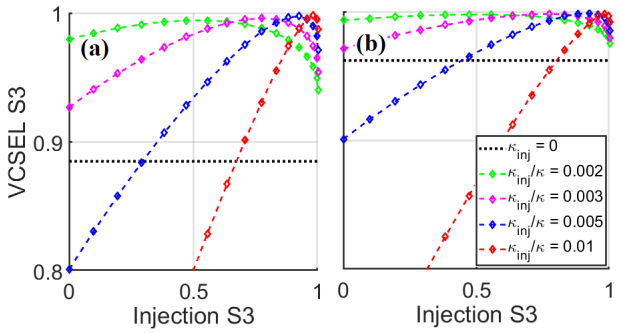

Fig. 9. SFM VCSEL S3 versus injection S3 with varying injection magnitude and reduced birefringence (a) $\gamma_p = 0.2ns^{-1}, S3_{pump} = 0.25$ (b) $\gamma_p = 0.2ns^{-1}, S3_{pump} = 0.38$.

An analysis of the VCSEL ellipticity with linear and spin-polarised pumping and optical injection has found a dependence on the injection rate and birefringence. For linear pumping, steady state analysis of the SFM shows that a particular κ_{inj}/κ value (or correspondingly $\tilde{E}_{inj}/\tilde{E}$) produces circular solutions for the injected VCSEL system. The results show also that finite birefringence shifts a sinusoidal VCSEL ellipticity peak towards the higher frequency axis, in accordance with results from the experiment and SFM.

The output-input ellipticity of the system shows unique nonlinear relationships. The parameters used in the SFM show that some of these responses can be tailored by changes in simple operational conditions e.g. relative injection strength, but others are reliant on selection of materials e.g. birefringence and spin relaxation rates. This suggests that with further exploitation of polarisation to encode data [13] these ellipticity properties might also be used, exploiting the unique spin coupling between electrons and photons in spin VCSELs. The varied ellipticity responses may have applications in logic operations and/or signal processing. For example, the approximately symmetrical peak for $\kappa_{inj}/\kappa = 0.02$ (red line) in figure 8a may form the basis for an XOR gate with the right discrimination levels; the peaks skewed to higher $S3_{inj}$ from higher injection coupling may form an AND or OR gate (e.g. blue lines figure 8a,b, red lines figure 9); and the peaks skewed towards zero $S3_{inj}$ a NOR gate (black line figure 8a, red line figure 8b).

High values of the relative output to input ellipticity can be achieved under spin polarised pumping (figures 6, 9). This is similar to spin amplification of the pump, but requires much lower input power, demonstrating a potential application for regeneration of circularly polarised signals in future telecommunications systems. Furthermore, reduced birefringence (figure 6b, 9), which is feasible considering recent developments [35], [38]–[43] would give a very high output ellipticity for any input ellipticity or ψ_{inj}, creating a signal spin regenerator robust to the input polarisation state. Metamaterials [44]–[46], or other exotic materials such as chiral conjugated polymer films [47] have recently been investigated which can generate elliptic from linear polarisation. However, spin VCSELs also offer optical amplitude gain in addition to their polarisation responses. Such benefits are predicted for fairly modest spin–polarised pumping ($S3_{pump} = 0.25$ and 0.38 figure 9) and γ_s values consistent with current materials at room temperature. Values of this order may be achievable with spin-aligning electrical contacts [2], [48] for future applications.

VI. CONCLUSIONS

We have demonstrated two types of pump-VCSEL polarisation response in a solitary spin VCSEL, depending on the magnitudes and signs of α, γ_a and γ_p. We have furthermore shown a range of output (VCSEL) versus input (optical injection) ellipticity responses depending on the injection magnitude and angle. Steady-state analysis based on the SFM for the case of linear pump and injection ellipticity supports the results. We have described how these novel output-input ellipticity responses, which can be tailored by choice of $\gamma_p, S3_{pump}$ and $S3_{inj}$, may be exploitable in logic or signal processing operations using only the ellipticity. High values of output ellipticity have been demonstrated for linear pumping under particular conditions, and more robustly with spin polarised pumping, with the former achievable in a non-spin laser, and the latter achievable with spin aligning electrical contacts or optical pumping.

APPENDIX
CONVERSION BETWEEN COMPLEX FIELD AND STOKES PARAMETERS

A. Stokes Parameters From Complex Linearly Polarized Fields

The Stokes parameters can be written in terms of the complex fields $\tilde{E}_x = |\tilde{E}_x|\exp(i\phi_x)$, $\tilde{E}_y = |\tilde{E}_y|\exp(i\phi_y)$ and phase difference $\phi = \phi_y - \phi_x$ as [49]

$$S1 = \left(|\tilde{E}_x|^2 - |\tilde{E}_y|^2\right) / \left(|\tilde{E}_x|^2 + |\tilde{E}_y|^2\right) \quad \text{(A1)}$$

$$S2 = 2|\tilde{E}_x||\tilde{E}_y|\cos\phi / \left(|\tilde{E}_x|^2 + |\tilde{E}_y|^2\right) \equiv 2Re(\tilde{E}_x^*\tilde{E}_y) / \left(|\tilde{E}_x|^2 + |\tilde{E}_y|^2\right) \quad \text{(A2)}$$

$$S3 = -2|\tilde{E}_x||\tilde{E}_y|\sin\phi / \left(|\tilde{E}_x|^2 + |\tilde{E}_y|^2\right) \equiv -2Im(\tilde{E}_x^*\tilde{E}_y) / \left(|\tilde{E}_x|^2 + |\tilde{E}_y|^2\right) \quad \text{(A3)}$$

Note the change of sign for equation (A3) compared to equation (6.1-9d) in [48] due to the circular polarisation convention used (here $\phi = -, +\pi/2$ for RCP,LCP, $\phi = +, -\pi/2$ for RCP,LCP in [49]).

Using the Stokes parameters from (A1) – (A3), ψ can be generated using equation (5).

B. Complex Injection Fields From Stokes Parameters

We use a normalisation of the injection fields so that $|\tilde{E}_{inj,x}|^2 + |\tilde{E}_{inj,y}|^2 = S1^2 + S2^2 + S3^2 = 1$. Firstly from (1) and (2), $S1_{inj}, S2_{inj}$ are generated from $S3_{inj}, \psi_{inj}$ as (A4), (A5), noting that $-\pi \leq 2\psi_{inj} \geq \pi$ and $-\pi/2 \leq 2\chi \geq \pi/2$.

$$S1_{inj} = \sqrt{1 - S3_{inj}^2}\cos 2\psi_{inj} \quad \text{(A4)}$$

$$S2_{inj} = \sqrt{1 - S3_{inj}^2}\sin 2\psi_{inj} \quad \text{(A5)}$$

From (A1)

$$|\tilde{E}_{x,inj}| = \sqrt{(1 + S1_{inj})/2} \tag{A6}$$

$$|\tilde{E}_{y,inj}| = \sqrt{(1 - S1_{inj})/2} \tag{A7}$$

From (A2) and (A3) the phase difference ϕ_{inj} can be derived as (A8), using the 4-quadrant atan2 function and noting that both $S3_{inj}$ and $S3_{inj}$ are signed values. Care is needed as (A8) is undefined for $S2_{inj}$ of exactly zero, so ϕ_{inj} cannot be derived for $S2_{inj} = 0$ when *both* $S1_{inj}$ and $S3_{inj}$ are finite (if either $S1_{inj}$ or $S3_{inj}$ are unity, ϕ_{inj} is directly apparent as $\mathbb{Z}\pi$ or $\mathbb{Z}\pi/2$). This also applies to other forms for ϕ e.g. using (6.1-6)-(6.1.7) from [49], however, ϕ_{inj} can be derived numerically in this situation.

$$\phi_{inj} = \tan^{-1}\left(-\frac{S3_{inj}}{S2_{inj}}\right) \tag{A8}$$

Noting that the Stokes parameters contain only the relative phase difference, there exists an infinite combination of absolute phases $\phi_{y,inj}$,$\phi_{x,inj}$ that form a particular relative phase $\phi_{inj} = \phi_{y,inj} - \phi_{x,inj}$. To generate the complex injection fields, we choose the Jones vectors convention that the phase of $\tilde{E}_{x,inj}$ is zero, therefore $\tilde{E}_{x,inj} \equiv |\tilde{E}_{x,inj}|$, $\tilde{E}_{y,inj} = |\tilde{E}_{y,inj}| exp(i\phi_{inj})$.

References

[1] J. Rudolph and D. Hägele, "Laser threshold reduction in a spintronic device," *Appl. Phys. Lett.*, vol. 82, no. 25, pp. 4516–4518, Jun. 2003.

[2] M. Holub, J. Shin, D. Saha, and P. Bhattacharya, "Electrical spin injection and threshold reduction in a semiconductor laser," *Phys. Rev. Let.*, vol. 98, no. 14, Apr. 2007, Art. no. 146603.

[3] F.-k. Hsu, W. Xie, Y.-S. Lee, S.-D. Lin, and C.-W. Lai, "Ultrafast spin-polarized lasing in a highly photoexcited semiconductor microcavity at room temperature," *Phys. Rev. B, Condens. Matter*, vol. 91, May 2015, Art. no. 195312.

[4] B. Cemlyn *et al.*, "Near-threshold high spin amplification in a 1300 nm GaInNAs spin laser," *Semicond. Sci. Technol.*, vol. 33, no. 9, Aug. 2018, Art. no. 094005.

[5] N. Gerhardt, S. Hovel, M. Hofmann, J. Yang, D. Reuter, and A. Wieck, "Enhancement of spin information with vertical cavity surface emitting lasers," *Electron. Lett.*, vol. 42, no. 2, pp. 88–89, Jan. 2006.

[6] S. Hovel, A. Bischoff, N. Gerhardt, M. Hofmann, T. A. Kroner, and R. Michalzik, "Optical spin manipulation of electrically pumped vertical-cavity surface-emitting lasers," *Appl. Phys. Lett.*, vol. 92, Jan. 2008, Art. no. 041118.

[7] K. Schires *et al.*, "Optically-pumped dilute nitride spin-VCSEL," *Opt. Express*, vol. 20, no. 4, pp. 3550–3555, Jan. 2012.

[8] S. Hovel, N. Gerhardt, M. Hofmann, J. Yang, D. Reuter, and A. Wieck, "Spin controlled optically pumped vertical cavity surface emitting laser," *Electron. Lett.*, vol. 41, no. 5, pp. 251–253, Mar. 2005.

[9] H. Höpfner, M. Lindemann, N. Gerhardt, and R. Hofmann, "Controlled switching of ultrafast circular polarization oscillations in spin-polarized vertical-cavity surface-emitting lasers," *Appl. Phys. Lett.*, vol. 104, Jan. 2014, Art. no. 022409.

[10] M. Lindemann, H. Höpfner, N. C. Gerhardt, M. R. Hoffman, T. Pusch, and R. Michalzik, "Ultrafast polarization dynamics with controlled polarization oscillations in vertical-cavity surface-emitting lasers," *Proc. SPIE, Vertical-Cavity Surf.-Emitting Lasers XIX*, vol. 9381, Mar. 2015, Art. no. 93810I. doi: 10.1117/12.2076920.

[11] M. Li, H. Jähme, H. Soldat, N. C. Gerhardt, M. R. Hofmann, and T. Ackemann, "Birefringence controlled room-temperature picosecond spin dynamics close to the threshold of vertical-cavity surface-emitting laser devices," *Appl. Phys. Lett.*, vol. 19, Sep. 2010, Art. no. 191114.

[12] M. Lindemann, N. C. Gerhardt, M. R. Hofmann, T. Pusch, and R. Michalzik, "Influence of birefringence splitting on ultrafast polarization oscillations in VCSELs," *Proc. SPIE, Vertical-Cavity Surf.-Emitting Lasers XX*, vol. 9766, Mar. 2016, Art. no. 97660L. doi: 10.1117/12.2212413.

[13] M. Lindemann, T. Pusch, R. Michalzik, N. C. Gerhardt, and M. R. Hofmann, "Spin lasers for optical data communication," *Proc. SPIE, Semicond. Lasers Laser Dyn. VIII*, vol. 10682, May 2018, Art. no. 1068205. doi: 10.1117/12.2306464.

[14] N. Li, H. Susanto, B. Cemlyn, I. D. Henning, and M. J. Adams, "Secure communication systems based on chaos in optically pumped spin-VCSELs," *Opt. Lett.*, vol. 42, no. 17, pp. 3494–3497, Sep. 2017.

[15] N. Khan, K. Schires, A. Hurtado, I. D. Henning, and M. J. Adams, "Current-dependence of polarisation switching and locking in an optically injected 1550 nm vertical-cavity surface-emitting laser," *IET Optoelectron.*, vol. 5, no. 3, pp. 110–113, Jun. 2011.

[16] M. Jadan, J. S. Addasi, L. I. Burov, A. S. Gorbatsevich, and P. M. Lobatsevich, "Polarization switching mechanism in surface-emitting semiconductor lasers," *Optik*, vol. 158, pp. 118–126, Apr. 2018.

[17] N. A. Khan, K. Schires, A. Hurtado, I. D. Henning, and M. J. Adams, "Temperature dependent dynamics in a 1550-nm VCSEL subject to polarized optical injection," *IEEE J. Quantum Electron.*, vol. 48, no. 12, pp. 712–719, May 2012.

[18] C. Jun, C. Jian-Jun, W. Zheng-Mao, J. Bo, and X. Guang-Qiong, "Investigations on the polarization switching and bistability in a 1550 nm vertical-cavity surface-emitting laser under variable-polarization optical injection," *Acta Phys. Sinica*, vol. 65, Aug. 2016, Art. no. 164204.

[19] D. Hayashi, K. Nakao, T. Katayama, and H. Kawaguchi, "All-optical 2-bit header recognition and packet switching using polarization bistable VCSELs," *Opt. Express*, vol. 23, no. 7, pp. 8357–8364, Mar. 2015.

[20] T. Katayama, D. Hayashi, and H. Kawaguchi, "All-optical shift register using polarization bistable VCSEL array," *IEEE Photon. Technol. Lett.*, vol. 28, no. 19, pp. 2062–2065, Oct. 1, 2016.

[21] T. Katayama, K. Nakao, D. Hayashi, and H. Kawaguchi, "Flip-flops using polarization bistable VCSEL with AND-gate functionality by two wavelength inputs," *IEICE Electron. Express*, vol. 13, no. 5, Feb. 2016, Art. no. 20160064. doi: 10.1587/elex.13.20160064.

[22] H. Kawaguchi, "Polarization-bistable VCSELs and their applications for all-optical signal processing," in *Proc. 15th Int. Conf. Transparent Opt. Net (ICTON)*, Cartagena, Spain, Jun. 2013, pp. 23–27.

[23] S. Perrone, R. Vilaseca, and C. Masoller, "Stochastic logic gate that exploits noise and polarization bistability in an optically injected VCSEL," *Opt. Express*, vol. 20, no. 12, pp. 22692–22699, Sep. 2012.

[24] A. Quirce, J. R. Cuesta, A. Valle, A. Hurtado, L. Pesquera, and M. J. Adams, "Polarization bistability induced by orthogonal optical injection in 1550-nm multimode VCSELs," *IEEE J. Sel. Topics Quantum Electron.*, vol. 18, no. 2, pp. 772–778, Mar. 2012.

[25] M. F. Salvide, C. Masoller, and M. S. Torre, "All-optical stochastic logic gate based on a VCSEL with tunable optical injection," *IEEE J. Quantum Electron.*, vol. 40, no. 10, pp. 886–893, Oct. 2013.

[26] D. Zhong, Y. Ji, and W. Luo, "Controllable optoelectric composite logic gates based on the polarization switching in an optically injected VCSEL," *Opt. Express*, vol. 23, no. 23, pp. 29823–29833, Nov. 2015.

[27] R. Al-Seyab, K. Schires, N. A. Khan, A. Hurtado, I. D. Henning, and M. J. Adams, "Dynamics of Polarized Optical Injection in 1550-nm VCSELs: Theory and experiments," *IEEE J. Sel. Topics Quantum Electron.*, vol. 17, no. 5, pp. 1242–1249, Sep. 2011.

[28] A. A. Qader, Y. Hong, and K. A. Shore, "Lasing characteristics of VCSELs subject to circularly polarized optical injection," *J. Lightw. Technol.*, vol. 29, no. 24, pp. 3804–3809, Dec. 15, 2011.

[29] R. Al-Seyab, K. Schires, N. Khan, A. Hurtado, I. D. Henning, and M. J. Adams, "Dynamics of VCSELs subject to optical injection of arbitrary polarization," *IEEE J. Sel. Topics Quantum Electron.*, vol. 19, no. 4, Jan./Aug. 2013, Art. no. 1700512.

[30] S. Alharthi *et al.*, "Control of emitted light polarization in a 1310 nm dilute nitride spin-vertical cavity surface emitting laser subject to circularly polarized optical injection," *Appl. Phys. Lett.*, vol. 105, Nov. 2014, Art. no. 181106.

[31] S. Alharthi, A. Hurtado, V. Korpijarvi, M. Guina, I. Henning, and M. J. Adams, " Circular polarization switching and bistability in an optically injected 1300 nm spin-vertical cavity surface emitting laser," *Appl. Phys. Lett.*, vol. 106, Jan. 2015, Art. no. 021117.

[32] N. Volet, "Theory and characterization of elliptically polarized modes in vertical-cavity surface-emitting lasers," *Proc. SPIE, Vertical-Cavity Surf.-Emitting Lasers XIX*, vol. 9381, Mar. 2015, Art. no. 93810U. doi: 10.1117/12.2078641.

[33] T. Jouhti *et al.*, "Dilute nitride vertical-cavity surface-emitting lasers," *New J. Phys.*, vol. 5, p. 84, Jul. 2003.

[34] M. Sciamanna and K. Panajotov, "Two-mode injection locking in vertical-cavity surface-emitting lasers," *Opt. Lett.*, vol. 30, no. 21, pp. 2903–2905, Nov. 2005.

[35] T. Fördös *et al.*, "Eigenmodes of spin vertical-cavity surface-emitting lasers with local linear birefringence and gain dichroism," *Phys. Rev. A, Gen. Phys.*, vol. 96, Oct. 2017, Art. no. 043828.
[36] M. Adams, N. Li, B. Cemlyn, H. Susanto, and I. Henning, "Algebraic expressions for the polarisation response of spin-VCSELs," *Semicond. Sci. Technol.*, vol. 33, Mar. 2018, Art. no. 064002.
[37] H. Susanto, K. Schires, M. J. Adams, and I. D. Henning, "Spin-flip model of spin-polarized vertical-cavity surface-emitting lasers: Asymptotic analysis, numerics, and experiments," *Phys. Rev. A, Gen. Phys.*, vol. 92, Dec. 2015, Art. no. 063838.
[38] J. Frougier, G. Baili, I. Sagnes, D. Dolfi, J. George, and M. Alouini, "Accurate measurement of the residual birefringence in VECSEL: Towards understanding of the polarization behavior under spin-polarized pumping," *Opt. Express*, vol. 23, no. 8, pp. 9573–9588, Apr. 2015.
[39] N. Yokota, R. Takeuchi, H. Yasaka, and K. Ikeda, "Lasing polarization characteristics in 1.55- μm spin-injected VCSELs," *IEEE Photon. Technol. Lett.*, vol. 29, no. 9, pp. 711–714, May 1, 2017.
[40] M. Lindemann, T. Pusch, R. Michalzik, N. C. Gerhardt, and M. R. Hofmann, "Frequency tuning of polarization oscillations: Toward high-speed spin-lasers," *Appl. Phys. Lett.*, vol. 108, Jan. 2016, Art. no. 042404.
[41] C. M. Long *et al.*, "Polarization mode control of long-wavelength VCSELs by intracavity patterning," *Opt. Express*, vol. 24, no. 9, pp. 9715–9722, May 2016.
[42] A. Joly *et al.*, "Compensation of the residual linear anisotropy of phase in a vertical-external-cavity-surface-emitting laser for spin injection," *Opt. Lett.*, vol. 42, no. 3, pp. 651–654, Feb. 2017.
[43] T. Fördös, K. Postava, H. Jaffrès, D. Q. To, J. Pištora, and H. J. Drouhin, "Mueller matrix ellipsometric study of multilayer spin-VCSEL structures with local optical anisotropy," *Appl. Phys. Lett.*, vol. 112, May 2018, Art. no. 221106.
[44] L. H. Nicholls *et al.*, "Ultrafast synthesis and switching of light polarization in nonlinear anisotropic metamaterials," *Nature Photon.*, vol. 11, no. 10, pp. 628–633, Sep. 2017.
[45] O. Altintas, E. Unal, and O. Akgol, "Design of a wide band metasurface as a linear to circular polarization converter," *Mod. Phys. Lett. B*, vol. 31, no. 30, Sep. 2017, Art. no. 1750274.
[46] Z. Li, W. Lu, H. Cheng, S. Chen, and J. Tian, "Realizing broadband and invertible linear-to-circular polarization converter with ultrathin single-layer metasurface," *Sci. Rep.*, vol. 5, Dec. 2015, Art. no. 18106.
[47] D. D. Nuzzo *et al.*, "High circular polarization of electroluminescence achieved via self-assembly of a light-emitting chiral conjugated polymer into multidomain cholesteric films," *ACS Nano.*, vol. 11, no. 12, pp. 12713–12722, Nov. 2017.
[48] G. Itskos, E. Harbord, S. K. Clowes, E. Clarke, L. Cohen, and R. Murray, "Oblique Hanle measurements of InAs/GaAs quantum dot spin-light emitting diodes," *Appl. Phys. Lett.*, vol. 88, Jan. 2006, Art. no. 022113.
[49] B. Saleh and M. Teich, "Fundamentals of photonics," in *Wiley Series in Pure and Applied Optics*, B. Saleh, Ed., 1st ed. Hoboken, NJ, USA: Wiley. 2007.

Benjamin R. Cemlyn received the B.Sc. degree in physics and the M.Sc. degree in electronic engineering from the University of Bristol, Bristol, U.K., in 2007 and 2008, respectively, and the Ph.D. degree in photonic integrated circuits from the University of Essex, Colchester, U.K., in 2013. In 2014, he joined the University of Bath, where he conducted research on mode locked lasers and optical fibers. Since 2015, he has been with the University of Essex, where he has been researching spin lasers, optical coupling, and waveguides. He is the author or a coauthor of numerous articles in areas including spin lasers, coupled lasers, photonic circuits, and quantum processes.

Ian D. Henning received the B.Sc. degree (Hons.) in applied physics and the Ph.D. degree from the University of Wales, Cardiff, U.K., in 1976 and 1979, respectively. In 1980, he joined the Devices Division, British Telecom Research Laboratories, Martlesham Heath, specializing in theory and measurements of semiconductor lasers. He has worked on optoelectronic devices and electronic/photonic device integration. He joined the Department of Electrical Systems Engineering, University of Essex, Colchester, U.K., in 2002, as a Professor. He is the author or a coauthor of numerous articles and two books. He is cited in ten patents.

Michael J. Adams received the Ph.D. degree in laser theory from the University of Wales, Cardiff, U.K., in 1970. Since 1996, he has been a Professor with the University of Essex, Colchester, U.K. He was involved in optoelectronics research and development with 15 years of experience in industry (Plessey, BT) and 34 years in academia (the University of Cardiff, the University of Southampton, and the University of Essex). He has published widely in the optoelectronics field over many years, including a standard text on optical waveguide theory and two books on semiconductor lasers and optical fibers for use in telecommunications. His current research interests include semiconductor lasers, optical amplifiers, optical waveguides, semiconductor nonlinear optics and optical switching devices, and nonlinear dynamics of lasers.

Edmund Harbord received the M.Phys. degree from the University of Oxford, Oxford, U.K., in 2002, and the M.Sc. degree in optics and photonics and the Ph.D. degree in spin dynamics in quantum dots from Imperial College London, London, U.K., in 2004 and 2009, respectively. He was a Researcher in nuclear spins and dark excitons in quantum dots with The University of Tokyo, Tokyo, Japan, from 2011 to 2013. Since 2013, he has been with the University of Bristol, Bristol, U.K., where he was a Researcher from 2013 to 2017 and has been a Lecturer in optical communications since 2017, with his research and publications focusing on nuclear and electron spin in quantum dots and quantum wells, single-photon sources, and associated quantum and classical optical physics. He received the Diawa scholarship in 2009.

Ruth Oulton received the M.Phys. degree from the Institute of Science and Technology, The University of Manchester, U.K., in 2000, and the Ph.D. degree in quantum dot spectroscopy from The University of Sheffield in 2003. From 2003 to 2006, she was an Alexander von Humboldt Fellow with TU Dortmund University, Germany, studying spin dynamics in quantum dots. Since 2018, she has been a Professor of quantum photonics with the University of Bristol. Her research interests cover a wide area of optical technologies, including electron, nuclear, and photon spin, single-photon sources, and quantum networks. In 2008, she became an EPSRC Career Acceleration Fellow.

Ville-Markus Korpijärvi received the M.Sc. degree in physics and the Ph.D. degree from the Tampere University of Technology, Tampere, Finland, in 2010 and 2015, respectively. He is currently a Process Development Engineer with Okmetic Oy, Helsinki, Finland. He has published widely on laser and optical device growth and fabrication technologies, and molecular beam epitaxy in particular. His research interests include dilute nitrides, high-power and spin-VCSELs, and thin films.

Mircea Guina received the Ph.D. degree in physics from the Tampere University of Technology, Tampere, Finland, in 2002. Since 2008, he has been a Professor of optoelectronics with Tampere University, where he currently leads the Optoelectronics Research Centre. He conducts research on several major topics, including molecular beam epitaxy of novel optoelectronic compounds, development of semiconductor lasers and high-efficiency solar cells, photonic integration, and use of lasers in medicine, LiDAR, and lensing. He is also a Co-Founder and the Chairman of three start-ups related to laser technologies: Vexlum Oy, Reflekron Oy, and Picophotonics Oy. He has authored or coauthored more than 180 journal articles, several book chapters, has given more than 35 invited talks at major international conferences, and holds four international patents. Recently, he was awarded the OSA Fellow and the SPIE Fellow distinctions for his work on various optoelectronics and laser technologies. He was a recipient of the ERC Advanced Grant for the development of high-efficiency solar cell technology (AMETIST). He is also a Topical Editor of the *Optics Letters* journal and the *Journal of the European Optical Society*.